Chinese Journal of
POLYMER SCIENCE

RESEARCH ARTICLE

https://doi.org/10.1007/s10118-026-3625-6
Chinese J. Polym. Sci.

A Simple Method for Evaluating Periodic Structures Based on Atomic Force Microscopy Images

Yun-Peng Li[a*], Wen-Ya Yuan[a], Bing-Hui Xu[a], Wei-Yu Li[a], Rui Xin[a], and Shou-Ke Yan[a,b]

[a] *Key Laboratory of Rubber-Plastics, Ministry of Education/Shandong Provincial Key Laboratory of Rubber-plastics, Qingdao University of Science and Technology, Qingdao 266042, China*
[b] *State Key Laboratory of Chemical Resource Engineering, Beijing University of Chemical Technology, Beijing 100029, China*

Electronic Supplementary Information

Abstract Small-angle X-ray scattering (SAXS), a conventional and widely accepted technique, has been frequently used to evaluate the periodic structure of semicrystalline polymeric materials. However, SAXA data interpretation relies heavily on intricate theoretical models and assumptions regarding the electron density profiles. In this study, we developed a simple image analysis method for calculating the sizes of both crystalline and amorphous regions, together with the long period, based on the images obtained *via* atomic force microscopy (AFM). This was confirmed by using melt-drawn poly(L-lactic acid) films composed of chain-folded lamellar crystals, and the long period obtained through image analysis (34.4 nm) was very close to that obtained by SAXS (34.9 nm), indicating the reliability of the method. The newly developed method can be used to analyze the structure of films with fibrillar crystals, and even with shish-kebab structures, through the accurate and effective separation of shish and kebab structures individually. Undoubtedly, this work is of great significance for establishing precise structure-property correlations and providing fundamental insights into polymer crystallization mechanisms.

Keywords Crystalline morphology; Image analysis; Lamellar thickness; Long period

Citation: Li, Y. P.; Yuan, W. Y.; Xu, B. H.; Li, W. Y.; Xin, R.; Yan, S. K. A simple method for evaluating periodic structures based on atomic force microscopy images. *Chinese J. Polym. Sci.* https://doi.org/10.1007/s10118-026-3625-6

INTRODUCTION

As is known to us, about 70% commercial polymers are crystalline materials. It is well documented that polymers crystallize, in most cases, through chain folding into a lamellar structure. Consequently, unlike organic and inorganic small molecules, polymers cannot fully crystallize, owing to the existence of chain folds and non-crystallizable parts due to stereo-defects of the molecular chains and their entanglement, and are thus referred to as semicrystalline polymers. In this case, polymer crystallization generally produces a lamellar structure comprising alternatively aligned crystalline lamellae and amorphous regions. Notably, the performance of polymeric materials, for example, the mechanical properties of engineering plastics, conductivity of conjugated polymers, and piezoelectricity of piezoelectric polymers, depends directly on the size and distribution of the crystalline and amorphous regions.[1–3] Therefore, quantitative analysis of crystalline and amorphous structures is needed to provide fundamental insights into the polymer crystallization mechanisms and to correlate the morphological structures with the properties. For this purpose, several sophisticated techniques have been developed to characterize the lamellar structure of polymers with respect to the size and distribution of the crystalline and amorphous regions. Among these techniques, small-angle X-ray scattering (SAXS) is a universal and widely accepted testing method that has been extensively applied to evaluate the long period.[4–10] Also the average lamellar thickness and width of the amorphous region between adjacent lamellae can be obtained using the one-dimensional correlation function method. It should be noted that the SAXS method (i) is optimally suited for systems with crystallinity either below 0.3 or above 0.7, but with challenges for ultrathin polymer films,[10] and (ii) cannot correlate the obtained results directly to real-space morphologies observed by microscopies, such as atomic force microscopy (AFM) and transmission electron microscopy (TEM). However, information about the long period and lamellar thickness cannot be directly obtained from AFM and TEM images. Taking these into account, the development of a new method for analyzing the average width of alternating crystalline and amorphous regions along with long period based on real-space morphological features in AFM images or TEM micrographs is of great significance, as it can offer a groundbreaking approach to correlate multiscale structural features with macroscopic properties.

In this work, we developed a novel image processing and analysis method for evaluating the long period and sizes of

* Corresponding author, E-mail: ypli@qust.edu.cn
Received January 21, 2026; Accepted February 12, 2026; Published online April 9, 2026

both crystalline and amorphous regions in polymeric materials based on AFM phase images. Considering the highly oriented poly(L-lactic acid) (PLLA) ultrathin film as a model system, the long period estimated by our newly developed imaging analysis method (*ca*. 34.4 nm) showed excellent consistency with that derived from SAXS (approximately 34.9 nm). In addition, this method can also be used to analyze and calculate the long period and sizes of the crystalline and amorphous regions of thin films with fibrillar crystals or shish-kebab structures, demonstrating its robustness and universality.

EXPERIMENTAL

Materials

PLLA with a weight-average molecular weight (M_w) of 2.2×10^5 g/mol and an optical purity of 95% was purchased from Changchun SinoBiomaterials Co., Ltd., (China). Polyethylene (PE) (M_w=9.9×10^4 g/mol) was supplied by Beijing Chemical Reagent Co., Ltd. *N*,*N*-dimethylformamide (DMF) and xylene were purchased from Sinopharm Chemical Reagent Co., Ltd.

Sample Preparation

Highly oriented PLLA and PE films have frequently been used in our previous works,[11–21] and their preparation procedures are briefly described here. They were prepared using the melt-draw technique proposed by Petermann and Gohil.[22] Melt-drawn PLLA and PE films were fabricated by spreading small amount of PLLA (0.6 wt% in DMF) or PE (0.5 wt% in xylene) solutions onto the preheated glass plates at 170 °C for PLLA and 140 °C for PE first, and then picking up the thin molten PLLA or PE layer by a motor-drive cylinder at draw speeds of 25 cm/s for PLLA and 5 cm/s for PE after evaporation of solvent, respectively.

To prepare highly oriented PE films with fibril structures, the as-prepared melt-drawn PE films were further stretched along the molecular chain direction to the draw ratios (λ) of 2 and 3.[21] In pursuit of this objective, a small amount of poly(acrylic acid) (PAA) aqueous solution (35 wt% of PAA) was dripped and blade-coated uniformly on a melt-drawn PE film supported by a silicon wafer. After dehumidification, the dried PAA thin layer thickening approximately 1 mm along with the melt-drawn PE film was detached from the silicon wafer and cut into rectangular strips (20 mm × 8 mm) for subsequent stretching. Stretching was performed at approximately 80 °C for softening the amorphous PAA layer to λ=2 and 3, then cooling down to room temperature, and finally wiping off the PAA layer by placing the strips with the PAA layer downward onto distilled water, that is, the PAA layer was directly in contact with water. After completely dissolving PAA through repeated water washing, the PE film floating on the water surface was transferred onto a silicon wafer for AFM analysis.

Characterizations

AFM characterization was performed using a Bruker Dimension Icon instrument operated in the tapping mode. Silicon tips with an Al coating, a resonance frequency of 300 kHz, and a spring constant of approximately 26 N/m were used. SAXS measurements were performed using a modified Xeuss 2.0 system (Xenocs, France) equipped with a semiconductor detector (Pilatus 300K, DECTRIS, Swiss). The wavelength of X-ray radiation was 0.15412 nm. The beam size is 1.2 mm × 1.2 mm, and the distance between the sample and detector is 2500 mm. The SAXS scattering pattern was collected over 1800 s in a vacuum environment and corrected using standard procedures.

Methodology

The fast Fourier transform (FFT), a fundamental method for time-domain to frequency-domain conversion, has been widely applied in signal processing, image analysis, and related computational sciences.[23,24] For an image containing periodic structural features, its frequency-domain image obtained through FFT processing provides the corresponding frequency signals in the normal direction of these periodic structures. By selectively filtering specific frequency components in the FFT image corresponding to the periodic structures of interest while suppressing others, inverse FFT (IFFT) can be reconstructed with enhanced time-domain representations of these structural features. This can effectively improve image quality, increase the signal-to-noise ratio, and highlight periodic features for further analysis.

RESULTS AND DISCUSSION

Image Processing Procedure

Fig. 1 presents the processing procedure of an AFM phase image with parallel aligned lamellar structure to evaluate the lamellar thickness, width of amorphous region and long period of it. Fig. 1(a) is an AFM phase image of PLLA melt-drawn film after successive annealing at 170 °C for 1 h, 150 °C for 0.5 h, 178 °C for 3 min, and 150 °C for 0.5 h, respectively, which has already been presented in a previous work and reproduced here with permission.[11] It shows well-defined and highly ordered structure with lamellae parallel to each other, and is ideal for the new developed method for quantitative evaluating the long period, lamellar thickness, and width of the amorphous region. To this end, the corresponding FFT image of Fig. 1(a) is first obtained as presented in Fig. 1(b), where four distinct frequency signal spots with central symmetry are observed, reflecting the highly ordered periodicity of the lamellar structure. To further enhance the periodic character of the layered structure, a rectangular mask has been used to the FFT image (Fig. 1b) for selectively emphasizing the four periodic signal spots, and thus obtaining clearer image for subsequent analysis (Fig. 1c). The four interested signal spots shown in Fig. 1(c) are then subjected to IFFT to reconstruct the spatial-domain image as shown in Fig. 1(d). For subsequent image processing requirements, the BGR color image shown in Fig. 1(d) needs to transform into an 8-bit grayscale image (Fig. 1e). The image in Fig. 1(e) should be then rotated to achieve vertical alignment of the highly ordered lamellae (Fig. 1f), after which a square region as shown in Fig. 1(g) has been cropped for further analysis. Following image binarization of Fig. 1(g) to generate Fig. 1(h), the resultant binary image (Fig. 1h) has been applied to quantitative structural analysis for determining the long period, lamellar thickness, and width of amorphous region using a custom-developed Python-based image analyzing algorithm. It should be mentioned that the binary image derived *via* FFT-masking-IFFT processing retains nearly all the periodic structures of the binary image of original image, while simultaneously filtering out the noise, as illustrated in Fig. S1 (in the electronic supplementary information,

ESI).

The logic and approach of the algorithm are briefly described below. In the long period analysis performed with Fig. 1(h), the length of every sequence of adjacent black and white pixels in each pixel line is measured, then transformed into the length in real space, and finally added to a list used for analyzing a long period from a statistical perspective. Similarly, when evaluating the thickness of crystalline domains or the width of amorphous regions, the length of every successive white or black pixel blocks was documented, transformed into the length in real space, and used to evaluate the lamellar thickness or the width of amorphous regions, respectively. The results obtained are shown in Fig. 2 as distribution histograms. Based on the Gaussian fitting analysis in Fig. 2, the width of the amorphous regions, lamellar thickness, and long period of the PLLA melt-drawn film are determined to be 9.8, 26.1 and 34.4 nm, respectively. Evidently, the sum of both the width of the amorphous regions and the thickness of the crystalline domains (35.9 nm) aligned well with the average value of the long period (34.4 nm). Moreover, it is clear that the calculated value of long period by AFM image (34.4 nm) is very close to that obtained by SAXS technique (34.9 nm), as shown in Figs. 3(a) and 3(b), underscoring the validity of the newly developed evaluation methodology. It should be noted that the resolution of the AFM images can affect the calculated values of the amorphous region width, lamellar thickness, and long period. We acquired a series of AFM images (presented in Fig. 1g) with resolutions ranging from 100 × 100 pixels to 2172 × 2172 pixels and subsequently calculated the width of amorphous regions, lamellar thickness, and long period for all images obtained in this manner. The corresponding results are shown in Fig. S2 (in ESI). It is evident that with increasing image resolution, the sizes of both the crystalline and amorphous regions, as well as the long period, exhibit an initial significant variation followed by a plateau stage. Constant fitting is performed on the data presented in

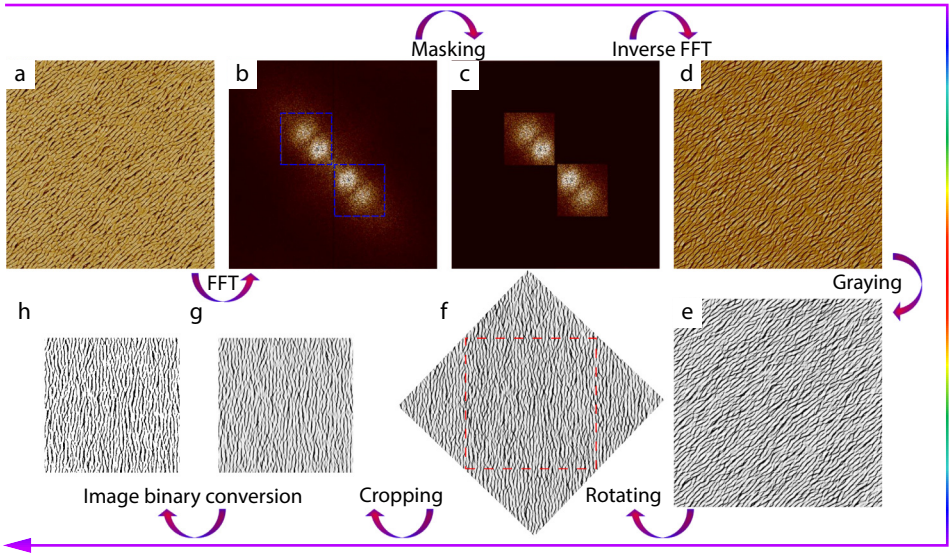

Fig. 1 Programming flowchart for evaluating the thickness of lamellae or width of crystalline domains, the width of amorphous regions and long period of oriented lamellar structure in semicrystalline polymer film based on AFM image. Part (a) is the AFM phase image of melt-drawn PLLA ultrathin film after annealing at 178 °C for 5 min and then 150 °C for 1 h (Reproduced from Ref. [11]; Copyright (2021), American Chemical Society). The scanning size of part (a) is 2 μm × 2 μm. Parts (b–h) show the results obtained by sequentially processing part (a) *via* (b) FFT processing, (c) masking, (d) IFFT processing, (e) grayscale conversion, (f) rotation, (g) cropping, and (h) binarization, respectively.

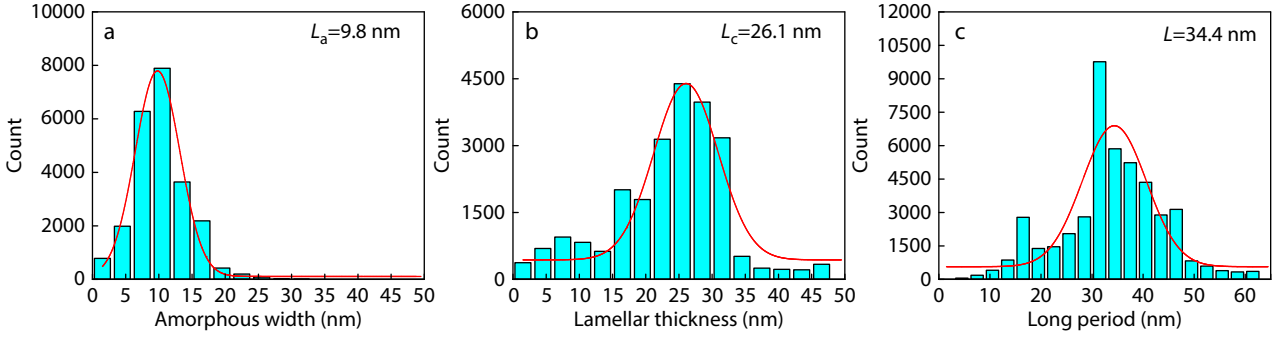

Fig. 2 The distribution histograms of the width of amorphous regions (a), thickness of crystalline domains (b) and long period (c) derived from AFM image described in Fig. 1 based on custom-developed image analyzing method. The red lines in parts (a), (b), and (c) represent Gaussian fits to the distribution histograms.

https://doi.org/10.1007/s10118-026-3625-6

Fig. S2 (in ESI), and the corresponding results are summarized in Table S1 (in ESI). These analyses demonstrate that the resolution at which the plateau begins (plateau onset resolution) for the amorphous region width, lamellar thickness, and long period is 193, 114, and 133 pixels, respectively. This indicates that the minimum resolution required to reliably calculate the width of amorphous regions, lamellar thickness, and long period from AFM images is 193 × 193 pixels. In addition, Fig. S2 and Table S1 (in ESI) clearly show that the mean value of the long period obtained *via* constant fitting is 34.95 nm, which exhibits excellent consistency with the value derived from SAXS (34.9 nm).

Analysis of Oriented Films with Fibrillar Crystals Based on Image Processing Method

It should be noted that unlike films with chain-folded lamellar crystals, the long period and widths of both crystalline and amorphous regions of samples with fibrillar crystals are unable to be characterized by SAXS technique. However, it can be ana-

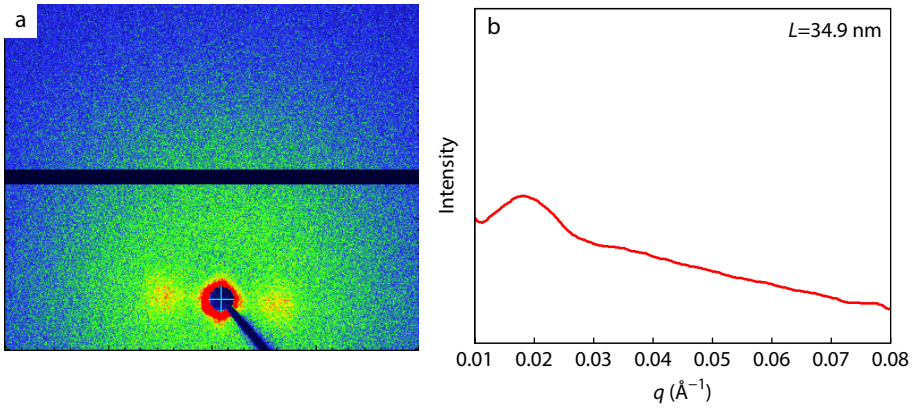

Fig. 3 Two-dimensional SAXS pattern (a) and corresponding one-dimensional SAXS curve (b) of the oriented PLLA film as used in Fig. 1(a).

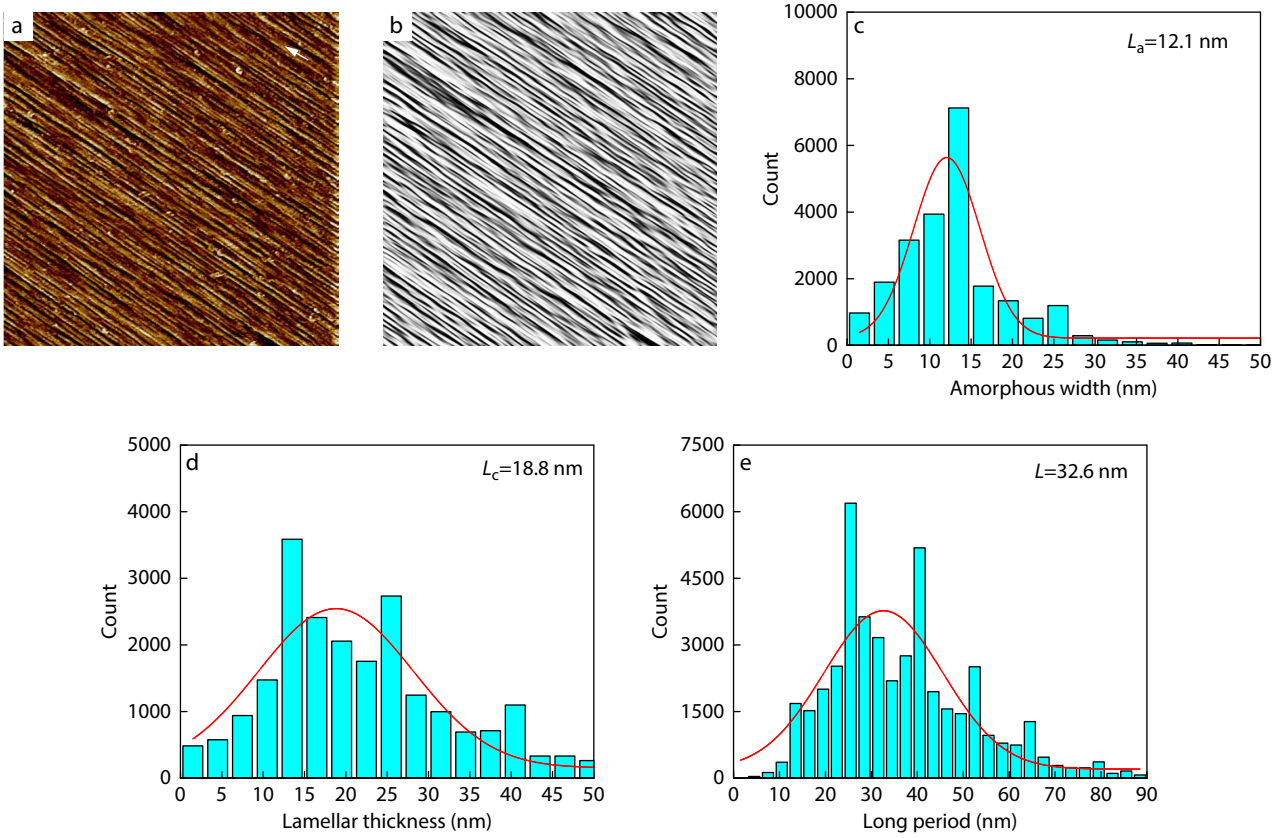

Fig. 4 AFM phase images of a PE melt-drawn ultrathin film further stretched along original chain orientation direction to λ=3 before (a) and after (b) FFT-masking-IFFT processing. The scanning size is 2 μm × 2 μm. The distribution histograms of the widths of amorphous (c) and crystalline (d) regions and corresponding long period (e) derived from part (b) based on custom-developed image processing method. The red lines in parts (c), (d), and (e) represent Gaussian fits to the distribution histograms. The white arrow in part (a) indicates the stretching direction of the melt-drawn PE ultrathin film. (a) is reproduced with permission from Ref. [21]; Copyright (2025), Elsevier Ltd.

https://doi.org/10.1007/s10118-026-3625-6

lyzed using the developed image-processing method. As an example, Fig. 4(a) shows an AFM phase image of an oriented polyethylene (PE) film containing predominantly fibrillar crystals, which was prepared by uniaxially stretching melt-drawn PE ultrathin films along its original molecular chain orientation direction to a draw ratio of λ=3.[21] The corresponding image generated by applying FFT-masking-IFFT processing to the image in Fig. 4(a) is shown in Fig. 4(b). It is obvious that Fig. 4(b) exhibits remarkable recovery of fibrillar crystal details after FFT-masking-IFFT processing and retains the fine structural features shown in Fig. 4(a). Based on the image analysis of Fig. 4(b), the width distribution histograms of amorphous regions and fibrillar crystals, together with long period are obtained and manifested in Figs. 4(c), 4(d) and 4(e), respectively. Gaussian fitting analysis yields the average values of 12.1, 18.8 and 32.6 nm for these respective parameters. According to a previous work,[21] it has been revealed that, except for the majority of oriented crystalline fibrils, there are also a minority of granular microcrystals in the PE film stretched along its molecular chain direction to λ=2, as shown in Fig. 5(a). The existence of these granular crystals may compromise the accuracy of width measurements for both fibrillar crystals and amorphous regions. To check the robustness of our developed evaluation method, the image shown in Fig. 5(a) was used to analyze and calculate the widths of both the crystalline and amorphous regions and the related long period. Fig. 5(b) shows the image obtained through the FFT-masking-IFFT processing of Fig. 5(a). With a close inspection, it is discovered that Fig. 5(b) strikingly recovers the structural details of the fibrillar crystal in Fig. 5(a) and meanwhile eliminating the granular microcrystals in Fig. 5(a). In this case, precise measurements of the widths of both fibrillar crystals and amorphous regions will not be influenced. Therefore, the width distributions of amorphous regions and fibrillar crystals, along with the long period distribution, were obtained through the analysis of Fig. 5(b), as shown in Figs. 5(c), 5(d) and 5(e), respectively. Gaussian fitting analysis gives the average values of 12.1, 17.2, and 33.6 nm for these parameters, respectively. Evidently, the widths of both crystalline and amorphous regions, as well as the long period derived from Figs. 4(a) and 5(a), are closely comparable, demonstrating the reliability and robustness of our developed image analysis approach.

Analysis of Shish-kebab Structure Based on Image Processing Method

For shish-kebab structures composed of fibrillar and chain-folded lamellar crystals, it is challenging to calculate the sizes of the crystalline and amorphous domains and long period because fibrillar crystals and lamellar crystals are aligned perpendicular to each other and mutually interfere. The newly developed image analysis approach can yet effectively analysis the "shish" and "kebab" parts in a shish-kebab structure, respectively. To demonstrate this, we selected an AFM phase image of a melt-

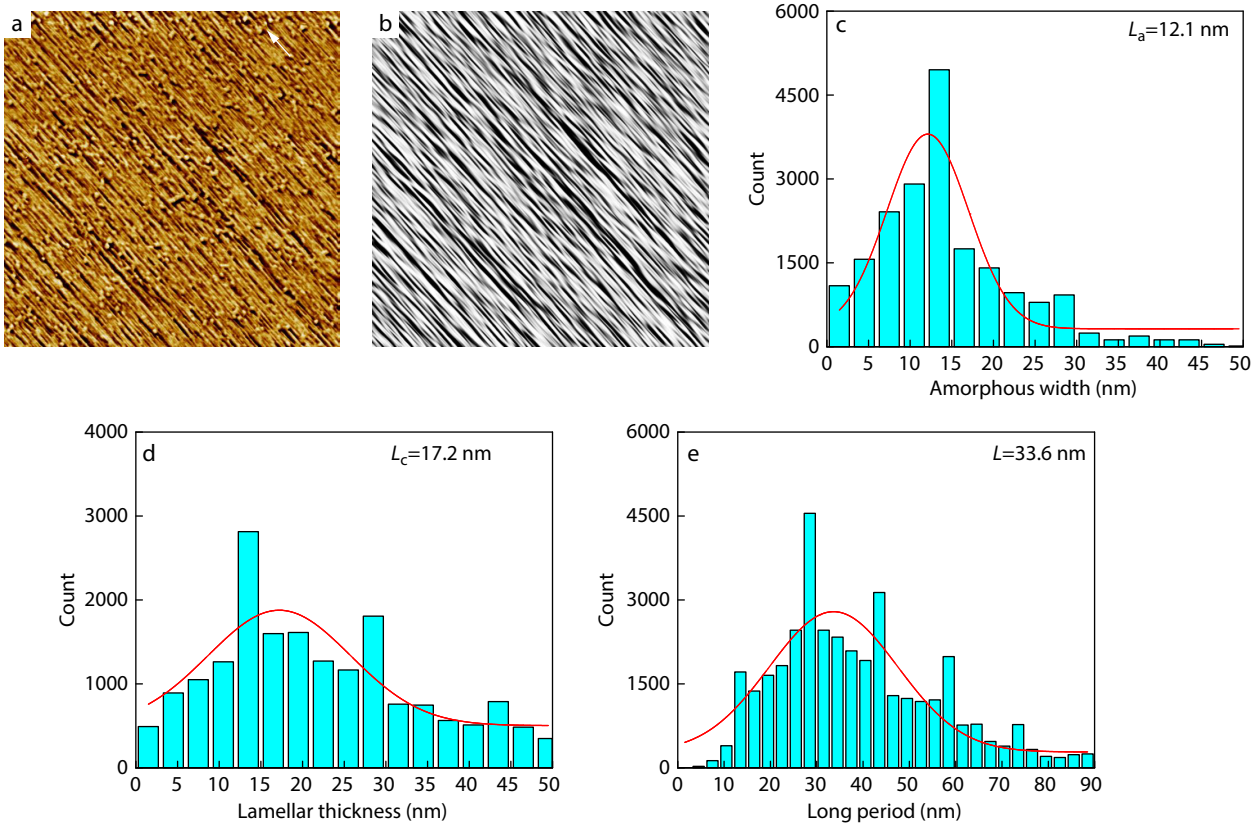

Fig. 5 AFM phase images of a PE melt-drawn ultrathin film further stretched along original chain orientation direction to λ=2 before (a) and after (b) FFT-masking-IFFT processing. The scanning size of part (a) is 2 μm × 2 μm. The distribution histograms of the widths of amorphous (c) and crystalline (d) regions and the corresponding long period (e) derived from part (b) based on custom-developed image processing method. The red lines in parts (c), (d), and (e) represent Gaussian fits to the distribution histograms. The white arrow in part (a) indicates the stretching direction of melt-drawn PE ultrathin film. (a) is reproduced with permission from Ref. [21]; Copyright (2025), Elsevier Ltd.

https://doi.org/10.1007/s10118-026-3625-6

drawn PE ultrathin film (Fig. 6a), which was previously confirmed to contain well-defined shish-kebab morphologies, as a representative sample.[21] Fourier transformation was applied to the AFM image to obtain the corresponding FFT image, as shown in Fig. 6(b). It is clear that the FFT image of the film with the shish-kebab structure shows two frequency signal spots (marked by blue dashed boxes) corresponding to the chain-folded lamellae, that is, the kebab structure, and two frequency signal streaks (indicated by red dashed boxes) related to the fibrillar crystals (*i.e.*, shish structure). The frequency signal spots in blue dashed boxes and frequency signal streaks in red dashed boxes are subsequently converted into spatial-domain images *via* IFFT separately, and thus visualizing the "kebab" and "shish" structures individually, as presented in Figs. 6(c) and 6(d), respectively. To check whether the structural details of original AFM phase image in Fig. 6(a) can be recovered or not, the IFFT images of the shish (Fig. 6d) and kebab (Fig. 6c) structures were integrated into a single fused image according to a pyramid image fusion method.[25] As shown in Fig. 7(a), the fused image preserves nearly all the fine structural details as the original AFM phase image in the grayscale mode (*cf.* Fig. 7b). This is more unambiguously confirmed by the movie shown in Movie S1 in ESI.

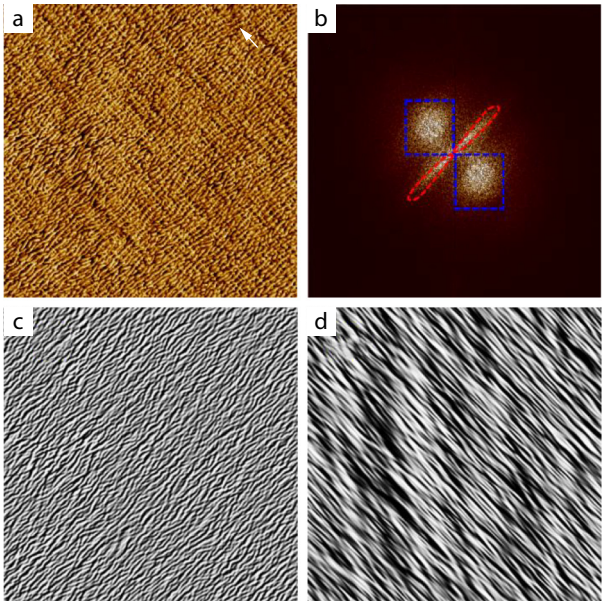

Fig. 6 The illustration showing the structure separation of chain folded lamellae and fibrillar crystals derived from (a) the AFM phase image of melt-drawn PE film. The scanning size of part (a) is 2 μm × 2 μm and the white arrow in part (a) indicates the drawing direction of melt-drawn PE film during preparation. AFM phase image is reproduced with permission from Ref. [21]; Copyright (2025), Elsevier Ltd. Part (b) presents the FFT image of part (a), in which the blue and red dashed boxes mark the frequency signals corresponding to the chain-folded lamellae and fibrillar crystals in part (a), respectively. Parts (c and d) are reconstructed *via* IFFT processing from the filtered frequency signals of the chain-folded lamellae and fibrillar crystals extracted from part (b).

The above results demonstrate that the image analysis method developed in this study can accurately and effectively separate the shish and kebab parts of a shish-kebab structure. In this case, the sizes of the crystalline domains and long period of both the chain-folded lamellae and fibrillar crystals can be analyzed and evaluated. Fig. 8 presents the distribution histograms of the width of amorphous regions (Fig. 8a), the thickness of chain-folded lamellae (Fig. 8b), and long period (Fig. 8c) obtained from the kebab structure image separated from the AFM phase image of melt-drawn PE shown in Fig. 6. Gaussian fitting results indicate the average values of 15.7, 16.0 and 29.7 nm for these parameters, respectively. It is worth mentioning that the long period measured perpendicular to the kebab structure from the AFM image (29.7 nm) is very close to that obtained by the SAXS results (27.9 nm) presented in Fig. S3 (in ESI), further demonstrating the validity of the newly developed methodology. Similarly, according to the shish structure image separated from the AFM phase image of melt-drawn PE, the widths of both amorphous regions and fibrillar crystals, together with long period are deter-

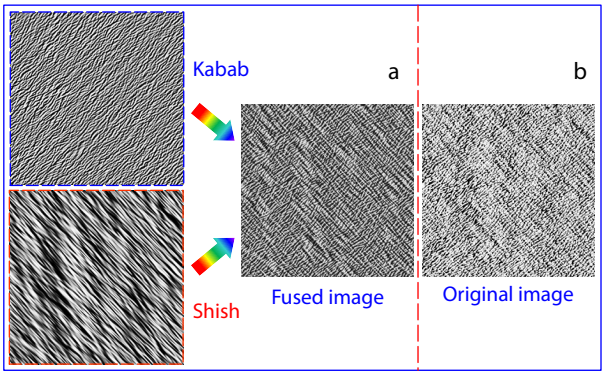

Fig. 7 (a) The integrated image derived from isolated chain folded lamellar and fibrillar crystal structures shown in Fig. 6 (a) and the original grayscale AFM phase image of melt-drawn PE film (b).

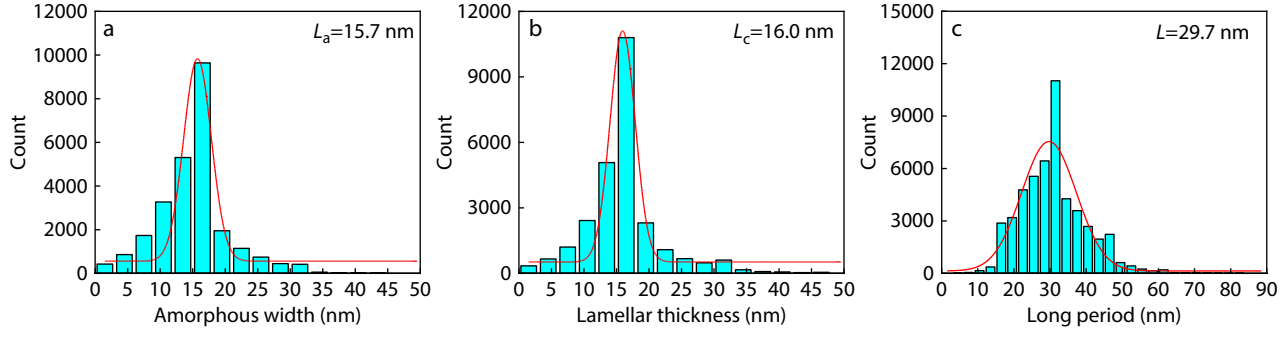

Fig. 8 The distribution histograms of the width of amorphous regions (a), the thickness of chain-folded lamellae (b), and long period (c) derived from the kebab structure image shown in Fig. 6(c).

https://doi.org/10.1007/s10118-026-3625-6

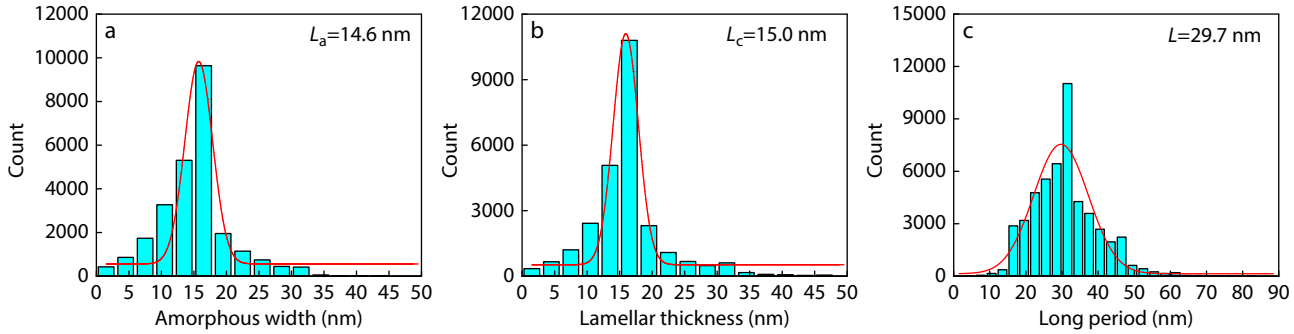

Fig. 9 The distribution histograms of the widths of amorphous (a) and crystalline (b) regions, and long period (c) derived from the shish structure image shown in Fig. 6(d).

mined as 14.6, 15.0 and 36.1 nm, respectively, as presented in Fig. 9. It is worth mentioning that the average width of the fibrillar crystals (measured perpendicular to the shish structure) in the melt-drawn PE film (15.0 nm) is slightly less than that in melt-drawn PE film further stretched to λ=2 (17.2 nm) and λ=3 (18.8 nm). This is reasonable and can be explained as follows. As the melt-drawn PE film is further stretched along its original molecular chain direction, the chain-folded PE lamellae undergo fragmentation followed by reorganization into fibrillar crystals, which finally results in an increase in the size of the fibrillar crystals.

CONCLUSIONS

In summary, an image analysis method for evaluating the sizes of both crystalline and amorphous regions, as well as long period of oriented semi-crystalline polymer film has been developed in this work. For the annealed PLLA melt-drawn film composed of well-defined chain-folded lamellar crystals, its long period evaluated by the imaging analysis method (34.4 nm) is very close to that derived from the SAXS results (34.9 nm). This method can also be used to estimate the average widths of both crystalline and amorphous regions as well as the long period of PE films with predominate fibrillar crystals. The results obtained for melt-drawn PE ultrathin films further stretched along the original chain orientation direction to λ=2 and 3 show that the widths of the fibrillar and amorphous regions, along with long period, of them are almost identical. In addition, it is unambiguously demonstrated that our developed method is applicable to the analysis of shish-kebab crystal structures through accurate and effective separation of the shish and kebab structures individually. It should be noted that AFM characterizes only the surface rather than the bulk crystallization morphologies. Therefore, the method described herein is only suitable for ultrathin film samples, since in such confined systems, the surface crystal morphology observed by AFM is representative of the overall sample structure. We hope that the developed method can be extended to the analysis of non-oriented structures and other multiscale structures by employing artificial intelligence and machine learning.

Conflict of Interests

Shou-Ke Yan is an associate editor for *Chinese Journal of Polymer Science* and was not involved in the editorial review or the decision to publish this article. The authors declare no interest conflict.

Electronic Supplementary Information

Movie revealing the similarity between the fused image and the original AFM image of the melt-drawn PE film. This information can be found at https://www.cjps.org/10.1007/s10118-026-3625-6.

Data Availability Statement

The data that support the findings of this study are available from the corresponding author upon reasonable request. Some of the source codes are available at https://github.com/liyunpeng1216/scientific-research. Please cite this work if you use these codes.

ACKNOWLEDGMENTS

This work was financially supported by the National Natural Science Foundation of China (No. 52403024) and the Qingdao Postdoctoral Foundation (No. QDBSH20240101014).

REFERENCES

1 Ma, B.; Wang, X.; He, Y.; Dong, Z.; Zhang, X.; Chen, X.; Liu, T. Effect of poly(lactic acid) crystallization on its mechanical and heat resistance performances. *Polymer* **2021**, *212*, 123280.
2 Guan, F.; Wang, J.; Pan, J.; Wang, Q.; Zhu, L. Effects of polymorphism and crystallite size on dipole reorientation in poly(vinylidene fluoride) and its random copolymers. *Macromolecules* **2010**, *43*, 6739–6748.
3 Biniek, L.; Leclerc, N.; Heiser, T.; Bechara, R.; Brinkmann, M. Large scale alignment and charge transport anisotropy of pBTTT films oriented by high temperature rubbing. *Macromolecules* **2013**, *46*, 4014–4023.
4 Hu, J.; Tashiro, K. Relation between higher-order structure and crystalline phase transition of oriented isotactic polybutene-1 investigated by temperature-dependent time-resolved simultaneous WAXD/SAXS measurements. *Polymer* **2016**, *90*, 165–177.
5 Qin, X.; Lu, Y.; Lyu, D.; Caton-Rose, F.; Coates, P.; Men, Y. Deformation temperature dependency of microstructure evolution in die-drawn *i*PP/UHMWPE blends. *Macromolecules*

Graphical Abstract

A Simple Method for Evaluating Periodic Structures Based on Atomic Force Microscopy Images

Yun-Peng Li, Wen-Ya Yuan, Bing-Hui Xu, Wei-Yu Li, Rui Xin, and Shou-Ke Yan

Qingdao University of Science and Technology; Beijing University of Chemical Technology

Small-angle X-ray scattering (SAXS) is widely used to characterize periodic structures in semicrystalline polymers but relies on complex models. We propose a simple atomic force microscopy (AFM) image-analysis method to measure crystalline, amorphous sizes and long period. The method can also analyze fibrillar and shish-kebab structures accurately.

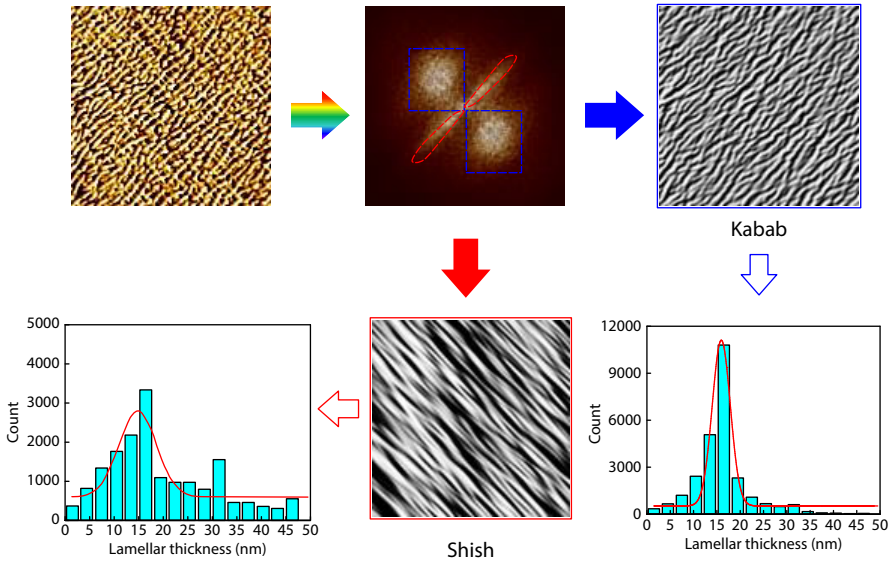

Chinese J. Polym. Sci., 2026 *https://doi.org/10.1007/s10118-026-3625-6*

2024, *57*, 9203–9215.

6 Wang, H.; Wu, C.; Cui, D.; Men, Y. Lamellar Thickness dependence of crystal modification selection in the syndiotactic polystyrene γ-to-α/β phase transition process. *Macromolecules* **2018**, *51*, 497–503.

7 Guo, H.; Zhu, J.; Li, C.; Zhao, C.; Cui, K.; Li, L. Strain rate dependence of amorphous phase instability in semicrystalline polymers: insights from the scale of lamellar stacks. *Macromolecules* **2024**, *57*, 4081–4094.

8 Yang, H.; Liu, D.; Ju, J.; Li, J.; Wang, Z.; Yan, G.; Ji, Y.; Zhang, W.; Sun, G.; Li, L. Chain deformation on the formation of shish nuclei under extension flow: an *in situ* SANS and SAXS study. *Macromolecules* **2016**, *49*, 9080–9088.

9 Chu, Z.; Liu, L.; Lou, Y.; Zhao, R.; Ma, Z.; Li, Y. Flow-induced crystallization of crosslinked poly(vinylidene fluoride) at elevated temperatures: formation and evolution of the electroactive β-phase. *Ind. Eng. Chem. Res.* **2020**, *59*, 4459–4471.

10 Strobl, G. R.; Schneider, M. Direct evaluation of the electron density correlation function of partially crystalline polymers. *J. Polym. Sci. Polym. Phys. Ed.* **1980**, *18*, 1343–1359.

11 Li, Y.; Xin, R.; Wang, S.; Guo, Z.; Sun, X.; Ren, Z.; Li, H.; Li, L.; Yan, S. Structure and mechanical property of melt-drawn oriented PLA ultrathin films. *Macromolecules* **2021**, *54*, 9124–9134.

12 Li, Y.; Wang, S.; Zhang, H.; Hu, J.; Liu, Q.; Xin, R.; Song, C.; Yan, S. Structure evolution of oriented poly(L-lactic acid) ultrathin films during deformation. *Macromolecules* **2022**, *55*, 6633–6643.

13 Li, Y.; Ma, M.; Xu, B.; Xin, R.; Yan, S. Impact of the exposure plane on the homoepitaxy of poly(L-lactic acid). *Macromolecules* **2025**, *58*, 4547–4554.

14 Li, Y.; Shen, H.; Wang, S.; Zhang, H.; Hu, J.; Xin, R.; Sun, X.; Yan, S. Impact of annealing on the melt recrystallization of a-PDLA/α-PLLA double-layered films. *Chinese J. Polym. Sci.* **2024**, *42*, 230–238.

15 Li, Y.; Shen, H.; Wang, S.; Zhang, H.; Hu, J.; Xin, R.; Yan, S. Structure evolution of amorphous poly(D-lactic acid) on highly oriented poly(L-lactic acid) film during annealing. *Polymer* **2023**, *280*, 126037.

16 Wang, J.; Liu, Y.; Li, H.; Yan, S.; Sun, X.; Tu, D.; Guo, X.; Ren, Z. Enhanced charge transport and thermoelectric performance of P(NDI2OD-T2) by epitaxial crystallization on highly oriented polyethylene substrates. *Mater. Chem. Front.* **2020**, *4*, 661–668.

17 Li, L.; Hu, J.; Li, Y.; Huang, Q.; Sun, X.; Yan, S. Evidence for the soft and hard epitaxies of poly(L-lactic acid) on an oriented polyethylene substrate and their dependence on the crystallization temperature. *Macromolecules* **2020**, *53*, 1745–1751.

18 Li, L.; Xin, R.; Li, H.; Sun, X.; Ren, Z.; Huang, Q.; Yan, S. Tacticity-dependent epitaxial crystallization of poly(L-lactic acid) on an oriented polyethylene substrate. *Macromolecules* **2020**, *53*, 8487–8493.

19 Jiang, T.; Wan, P.; Ren, Z.; Yan, S. Anisotropic polyaniline/SWCNT composite films prepared by in situ electropolymerization on highly oriented polyethylene for high-efficiency ammonia sensor. *ACS Appl. Mater. Interfaces* **2019**, *11*, 38169−38176.
20 Zhang, H.; Song, Y..; Li, N.; Wang, S..; Hu, J.; Xin, R.; Zhang, J.; Song, C.; Yan, S. Influence of freezing layer on the crystallization kinetics of PCL on oriented PE film. *Chinese J. Polym. Sci.* **2023**, *41*, 778−786.
21 Li, Y.; Ma, M.; Xu, B.; An, L.; Xin, R.; Yan, S. Reassessment of the epitaxial mechanism of poly(L-lactic acid) on polyethylene substrate. *Polymer* **2025**, *327*, 128389.
22 Petermann, J.; Gohil, R. M. A new method for the preparation of high modulus thermoplastic films. *J. Mater. Sci.* **1979**, *14*, 2260−2264.
23 Cooley, J. W.; Tukey, J. W. An algorithm for the machine calculation of complex fourier series. *Math. Comput.* **1965**, *19*, 297−301.
24 Gonzales, R. C.; Wintz, P. *Digital image processing*. Boston, Addison-Wesley Longman Publishing Co., Inc., **1987**.
25 Ma, J.; Ma, Y.; Li, C. Infrared and visible image fusion methods and applications: a survey. *Inform. Fusion.* **2019**, *45*, 153−178.

https://doi.org/10.1007/s10118-026-3625-6